

Applications of MLPG Method in Dynamic Fracture Problems

L. Gao¹, K. Liu^{1,2}, Y. Liu³

Abstract: A new numerical algorithm based on the Meshless Local Petrov-Galerkin approach is presented for analyzing the dynamic fracture problems in elastic media. To simplify the treatment of essential boundary condition, a novel modified Moving Least Square (MLS) procedure is proposed by introducing Lagrange multiplier into MLS procedure, which can perform both MLS approximation and interpolation in one approximation domain. The compact spline function is used as the test function in the local form of elasto-dynamic equations. For the feature of stress wave propagation, the coupled second-order ODEs respect to the time are solved by the explicit central difference method with lumped mass matrix. By adopting the modified MLS techniques, the essential boundary conditions can be simply introduced by direct row cross-out method. In order to improve the accuracy of this algorithm, quadratic basis and Gaussian weight function with a support domain larger than test functions are used in the approximation. Visibility criterion is used for presenting the discontinuous fields caused by cracks. The dynamic stress intensity factors in various modes are evaluated through a path-independent dynamic J' integral method, and the complicated diffractions of the stress waves near cracks are investigated in detail. The numerical results show that the present method is easy to implement, highly accurate and efficient for the problems considered.

keyword: Meshless Local Petrov-Galerkin method (MLPG); Modified moving least square; Wave propagation; Dynamic fracture; Crack modeling; Dynamic stress intensity factor (DSIF)

1 Introduction

Dynamic crack responses and propagation are important aspects of impact dynamics, and attract more and more scholars' interests due to the crucial need of wide-ranging engineering application and the research of many nature phenomena [Freund (1990); Rosakis and Ravichandran (2000)]. Stress wave propagation plays an important role in this study. Clarification of the mechanism of the interaction between transient wave propagation and cracks, defects or holes can help us in the design of complex structures and composite materials by acoustic emission, quantitative nondestructive materials testing, seismology applications and so on. Owing to the complication of these problems, the analytical results are always hard to be obtained. Thus, numerical simulation becomes an effective tool for analyzing such problems.

However, traditional numerical methods such as finite difference method, finite element method and finite boundary method, which are based on meshes, sometimes suffer from the difficulties of mesh discontinuity and distortion in the calculation of rapid dynamic fracture, plastic flow and fluid solid coupling problems, where large deformation often occurs. Although these difficulties can be partly solved by remeshing or mesh refinement, the complex algorithms for mesh treatments not only consumedly decrease the efficiency of computation, but also affect accuracy of the calculation results, even finally ruin the whole computational results.

In recent years, many meshless methods are introduced to overcome these drawbacks of mesh-based methods, such as SPH, EFG, FPM, Hp-Clouds Method, PUM, RKPM, MLPG, LBIE, RBF, PIM, BNM and so on. The summary of these newly developed meshless methods can be found in some key references [Belytschko, Krongauz, Organ, Fleming and Krysl (1996); Atluri and Shen (2002); Liu (2002); Li and Liu (2002); Atluri (2004); Atluri (2005)]. The common feature of meshless methods lies in that they all use weighted function with compact domain (also called window function in wavelet analysis) to construct unknown functions and fulfill interpolation or ap-

¹ State Key Laboratory for Turbulence and Complex Systems and Department of Mechanics and Engineering Science, Peking University, Beijing 100871, P R China

² Corresponding author. E-mail: kliu@pku.edu.cn

³ Institute of Mechanics, School of Civil Engineering, Beijing Jiaotong University, Beijing, 100044, P R China

proximation of variables through arbitrary arranged discrete nodes in the space without the topology information of the connections among them (namely mesh). These techniques include Kernel Approximation [Gingold and Moraghan (1977)], Moving Least Square (MLS) [Lancaster and Salkauskas (1981)], Partition of Unity (PU) [Melen and Babuska (1996)], Radial Based Function (RBF) [Powell (1992)] and so on. On the whole, meshless methods could be classified through the presentation of partial differential equations (PDEs) or the weighted residual method (WRM) [Atluri and Shen (2002); Liu (2002)]. Various newly developed meshless methods show more versatility, flexibility and capability than the traditional ones, although they are still immature in some aspects, and bring a new exciting prosperity to the whole field of scientific computation.

Among these meshless methods, MLPG approach, first proposed by Atluri and Zhu (1998), can be considered as a general framework for the other meshless methods. It provides the flexibility in choosing the trial and test functions, as well as the sizes and shapes of local sub-domains, and has been proved to be a truly meshless method [Atluri, Han and Rajendran (2004)]. It not only overcomes the problems that the traditional methods, which are based on the meshes, suffer from, but also brings forward some new methods with amazing flexibility and efficiency. By now, it has been successfully applied in analyzing both elasto-static and elasto-dynamic problems. Atluri and Zhu (2000) solved elasto-static problems. Lin and Atluri (2000) introduced the upwinding scheme to analyze steady convection-diffusion problems. Ching and Batra (2001) determined the crack tip fields in linear elasto-statics. Gu and Liu (2001) studied the forced vibrations of a beam. Long and Atluri (2002) solved the bending problem of a thin plate. Batra and Ching (2002) analyzed elasto-dynamic deformations near a crack/notch tip. Qian, Batra and Chen (2004) studied the static and dynamic deformations of the thick functionally graded elastic plate, etc. Han and Atluri (2004) extended this approach for solving 3-dimensional elasto-dynamics problems. For recent development of this approach, please refer to the references [Atluri (2004)] and [Atluri (2005)]. However, the applications of the MLPG method in the problems, such as the dynamic crack responses and propagation, have not been fully investigated. In addition, the efficiency and the accuracy of this method need to be further analyzed.

The purpose of this paper is to develop a new algorithm that further extends the MLPG method to analyze the stress wave propagation and dynamic fracture problems. In order to introduce essential boundary condition more directly and simply than general meshless methods by using MLS approximation, a new modified MLS procedure is proposed. The formulation for elasto-dynamics is discretized using MLPG1 approach. But the domains for the test functions and for the approximation are chose in different sizes. The coupled ODEs are integrated with respect to the time by the explicit central difference method with lumped mass matrix. The dynamic stress intensity factors near the crack tip are determined by using visible criterion and path independent dynamic J' integral. The availability of this algorithm in analyzing the dynamic response of cracks in various modes is discussed, respectively. Finally the complicated diffraction of the stress waves near a crack is investigated in detail.

2 MLPG formulation of elasto-dynamic equations

2.1 Governing equations

Considering a two-dimensional elasto-dynamic problem, the governing equations in Cartesian coordinates are written as

$$\begin{aligned}\sigma_{ij,j} + b_i &= \rho \ddot{u}_i \\ \sigma_{ij} &= D_{ijkl} \varepsilon_{kl} \\ \varepsilon_{ij} &= (u_{i,j} + u_{j,i})/2 \text{ in } \Omega \quad (i, j = 1, 2)\end{aligned}\quad (1)$$

where σ_{ij} and ε_{ij} are the stress and strain components, u_i and b_i the displacement and body force components, D_{ijkl} the elastic constants, ρ the mass density. The comma before an index represents partial space differentiation, and the dot notation is used to represent differentiation with respect to the time. The boundary and initial conditions are given as

$$\begin{aligned}u_i &= \bar{u}_i \quad \text{on } \Gamma_u \\ \sigma_{ij} n_j &= \bar{t}_i \quad \text{on } \Gamma_t \\ u_i(\mathbf{x}, 0) &= u_{0i}(\mathbf{x}) \\ \dot{u}_i(\mathbf{x}, 0) &= \dot{u}_{0i}(\mathbf{x})\end{aligned}\quad (2)$$

where \bar{u}_i are the prescribed displacement components on the essential boundary Γ_u . \bar{t}_i are the tractions on the natural boundary Γ_t . Γ_u and Γ_t present the complementary

parts of the whole boundary $\Gamma(\Gamma = \Gamma_u \cup \Gamma_f)$. $u_{0i}(\mathbf{x})$ and $\dot{u}_{0i}(\mathbf{x})$ are the prescribed initial displacement components and the velocity components, n_j the unit outward normal to the boundary Γ .

2.2 Modified MLS approximation

The MLS method of approximation is usually used in meshless approximation, due to its reasonable approximation accuracy with random data. However, for the shape functions obtained by the normal MLS procedure do not hold Kronecker delta property at nodes, special treatments, such as penalty method, modified variation principle method, Lagrange multiplier method and so on, are used to introduce essential boundary conditions in the procedure of the equation discretization. In this paper, we developed a new modified MLS, which can fulfill Kronecker delta property on essential boundary nodes.

The trial function $u_i^h(\mathbf{x}, t)$ at the point $\mathbf{x} = [x_1, x_2]^T$ for approximated displacement components over a 2D domain Ω_x is given as

$$u_i^h(\mathbf{x}, t) = \mathbf{p}^T(\mathbf{x}) \mathbf{a}_i(\mathbf{x}, t) \quad \mathbf{x} \in \Omega_x \quad (i = 1, 2) \quad (3)$$

where Ω_x is a sub-domain around the approximation point \mathbf{x} , $\mathbf{a}_i(\mathbf{x}, t)$ a vector of corresponding coefficient. $\mathbf{p}(\mathbf{x}) = [p_1(\mathbf{x}), p_2(\mathbf{x}), \dots, p_m(\mathbf{x})]^T$ is a complete basis vector, in which m is the number of terms in the basis. In present algorithm, polynomial basis are used. For linear basis,

$$\mathbf{p}(\mathbf{x}) = [1, x_1, x_2]^T \quad (m = 3) \quad (4)$$

and for quadratic basis,

$$\mathbf{p}(\mathbf{x}) = [1, x_1, x_2, x_1^2, x_1x_2, x_2^2]^T \quad (m = 6) \quad (5)$$

Assume that there are total N nodes in Ω_x . Differing from the normal MLS technique, these nodes are divided into two parts: N_{in} nodes satisfying MLS approximation condition, numbered as $1, \dots, N_{in}$, and $N_b = N - N_{in}$ nodes satisfying interpolation condition, numbered as $N_{in} + 1, \dots, N$. Thus, a modified functional J_i can be constructed by the summation of the weighted discrete L_2 norm of displacement components over the former part of $1, \dots, N_{in}$ nodes and the constrained conditions over the rest part of $N_{in} + 1, \dots, N$ nodes introduced by La-

grange multiplier, which is given as

$$J_i = \sum_{I=1}^{N_{in}} w(\mathbf{x} - \mathbf{x}_I) [\mathbf{p}^T(\mathbf{x}_I) \mathbf{a}_i(\mathbf{x}, t) - u_{iI}(t)]^2 + 2 \sum_{I=N_{in}+1}^N \lambda_{iI} [\mathbf{p}^T(\mathbf{x}_I) \mathbf{a}_i(\mathbf{x}, t) - u_{iI}(t)] \quad (6)$$

where \mathbf{x}_I denotes the position vector of node I , $u_{iI}(t)$ the fictitious values of displacement components on node I , $w(\mathbf{x} - \mathbf{x}_I)$ the weight function with the property of positive, compact, unity, decay about $|\mathbf{x} - \mathbf{x}_I|$ and delta function behavior as normal MLS weight functions, which could be Gaussian weight function

$$w(\mathbf{x} - \mathbf{x}_I) = \begin{cases} \frac{e^{-(|\mathbf{x}-\mathbf{x}_I|/c_I)^{2k}} - e^{-(r_I/c_I)^{2k}}}{1 - e^{-(r_I/c_I)^{2k}}} & |\mathbf{x} - \mathbf{x}_I| \leq r_I \\ 0 & |\mathbf{x} - \mathbf{x}_I| > r_I \end{cases} \quad (7)$$

or spline function

$$w(\mathbf{x} - \mathbf{x}_I) = \begin{cases} 1 - 6\left(\frac{|\mathbf{x}-\mathbf{x}_I|}{r_I}\right)^2 + 8\left(\frac{|\mathbf{x}-\mathbf{x}_I|}{r_I}\right)^3 - 3\left(\frac{|\mathbf{x}-\mathbf{x}_I|}{r_I}\right)^4 & 0 \leq |\mathbf{x} - \mathbf{x}_I| \leq r_I \\ 0 & |\mathbf{x} - \mathbf{x}_I| > r_I \end{cases} \quad (8)$$

where r_I is the radius of the influence domain for the weight function accompanied by node I , parameters c_I and k are used to control the shape of Gaussian weight function.

By minimizing weighted norm J_i over \mathbf{a}_i and combining with the constrain conditions, the following equations are obtained

$$\begin{cases} \frac{\partial J_i}{\partial \mathbf{a}_i} = 0 \\ \mathbf{p}^T(\mathbf{x}_I) \mathbf{a}_i(\mathbf{x}, t) = u_{iI}(t) \quad (I = N_{in} + 1, \dots, N) \end{cases} \quad (9)$$

Written in matrix form, the equations above change to

$$\begin{bmatrix} \mathbf{A}(\mathbf{x}) & \mathbf{P} \\ \mathbf{P}^T & \mathbf{0} \end{bmatrix} \begin{bmatrix} \mathbf{a}_i(\mathbf{x}, t) \\ \boldsymbol{\lambda}_i \end{bmatrix} = \begin{bmatrix} \mathbf{B}(\mathbf{x}) & \mathbf{0} \\ \mathbf{0} & \mathbf{I} \end{bmatrix} \begin{bmatrix} \mathbf{u}_i(t) \\ \mathbf{1} \end{bmatrix} \quad (10)$$

where

$$\mathbf{A}(\mathbf{x}) = \sum_{I=1}^{N_{in}} w(\mathbf{x} - \mathbf{x}_I) \mathbf{p}(\mathbf{x}_I) \mathbf{p}^T(\mathbf{x}_I)$$

$$\mathbf{B}(\mathbf{x}) = [w(\mathbf{x} - \mathbf{x}_1)\mathbf{p}(\mathbf{x}_1), w(\mathbf{x} - \mathbf{x}_2)\mathbf{p}(\mathbf{x}_2), \dots, w(\mathbf{x} - \mathbf{x}_{N_{in}})\mathbf{p}(\mathbf{x}_{N_{in}})]$$

$$\mathbf{P} = [\mathbf{p}(\mathbf{x}_{N_{in}+1}), \mathbf{p}(\mathbf{x}_{N_{in}+2}), \dots, \mathbf{p}(\mathbf{x}_N)] \quad (11)$$

The subscript values below the matrices in Eq. (10) denote the dimensions of these matrices. $\mathbf{u}_i(t) = [u_{i1}, u_{i2}, \dots, u_{iN}]^T$ is the generalized displacement vector with N nodes, $\boldsymbol{\lambda}_i = [\lambda_{i1}, \lambda_{i2}, \dots, \lambda_{iN_b}]^T$ is the Lagrange multiplier vector, $\mathbf{0}_{(N_b \times N_b)}$, $\mathbf{0}_{(m \times N_b)}$ and $\mathbf{0}_{(N_b \times N_{in})}$ are $N_b \times N_b$, $m \times N_b$ and $N_b \times N_{in}$ zero matrices, $\mathbf{I}_{(N_b \times N_b)}$ is a $N_b \times N_b$ identity matrix. It can be also written as

$$\begin{cases} \mathbf{A}(\mathbf{x})\mathbf{a}_i(\mathbf{x}, t) + \mathbf{P}\boldsymbol{\lambda}_i = \mathbf{B}(\mathbf{x})\mathbf{u}_{iin}(t) \\ \mathbf{P}^T\mathbf{a}_i(\mathbf{x}, t) = \mathbf{u}_{ib}(t) \end{cases} \quad (12)$$

where $\mathbf{u}_{iin}(t) = [u_{i1}, u_{i2}, \dots, u_{iN_{in}}]^T$ and $\mathbf{u}_{ib}(t) = [u_{iN_{in}+1}, u_{iN_{in}+2}, \dots, u_{iN}]^T$ are generalized displacement vectors for MLS approximation and interpolation conditions, respectively.

The coefficient $\mathbf{a}_i(\mathbf{x}, t)$ can be obtained as

$$\mathbf{a}_i(\mathbf{x}, t) = \mathbf{A}^{-1}(\mathbf{x})\{\mathbf{I} - \mathbf{P}(\mathbf{P}^T\mathbf{A}^{-1}(\mathbf{x})\mathbf{P})^{-1}\mathbf{P}^T\mathbf{A}^{-1}(\mathbf{x})\}\mathbf{B}(\mathbf{x})\mathbf{u}_{iin}(t) + \mathbf{P}(\mathbf{P}^T\mathbf{A}^{-1}(\mathbf{x})\mathbf{P})^{-1}\mathbf{u}_{ib}(t) \quad (13)$$

The trial function $u_i^h(\mathbf{x}, t)$ is rewritten as

$$u_i^h(\mathbf{x}, t) = \Phi^T(\mathbf{x})\mathbf{u}_i(t) \quad (14)$$

where $\Phi(\mathbf{x}) = [\phi_1, \phi_2, \dots, \phi_N]^T$ is the shape function vector given by

$$\Phi^T(\mathbf{x}) = \mathbf{p}^T(\mathbf{x}) \begin{bmatrix} \mathbf{S}(\mathbf{x})\mathbf{B}(\mathbf{x}) & \mathbf{Y}^T(\mathbf{x}) \\ (1 \times N) & (1 \times m) & (m \times N_{in}) & (m \times N_b) \end{bmatrix} \quad (15)$$

where

$$\mathbf{Y}(\mathbf{x}) = \mathbf{Q}^{-1}(\mathbf{x})\mathbf{P}^T\mathbf{A}^{-1}(\mathbf{x}) \quad (N_b \times m)$$

$$\mathbf{Q}(\mathbf{x}) = \mathbf{P}^T\mathbf{A}^{-1}(\mathbf{x})\mathbf{P} \quad (N_b \times N_b)$$

$$\mathbf{S}(\mathbf{x}) = \mathbf{A}^{-1}(\mathbf{x}) \begin{bmatrix} \mathbf{I} & -\mathbf{P}\mathbf{Y}(\mathbf{x}) \\ (m \times m) & (m \times m) \end{bmatrix} \quad (16)$$

The first derivations of this shape function over space variables x_i are obtained by

$$\Phi_{,i}^T(\mathbf{x}) = \mathbf{p}_{,i}^T(\mathbf{x}) \begin{bmatrix} \mathbf{S}(\mathbf{x})\mathbf{B}(\mathbf{x}) & \mathbf{Y}^T(\mathbf{x}) \\ +\mathbf{P}^T(\mathbf{x}) \begin{bmatrix} \mathbf{S}_{,i}(\mathbf{x})\mathbf{B}(\mathbf{x}) + \mathbf{S}(\mathbf{x})\mathbf{B}_{,i}(\mathbf{x}) & \mathbf{Y}_{,i}^T(\mathbf{x}) \end{bmatrix} \end{bmatrix} \quad (17)$$

where

$$\mathbf{p}_{,i}^T(\mathbf{x}) = [p_{1,i}(\mathbf{x}), p_{2,i}(\mathbf{x}), \dots, p_{m,i}(\mathbf{x})]$$

$$\mathbf{B}_{,i}(\mathbf{x}) = [w_{1,i}(\mathbf{x} - \mathbf{x}_1)\mathbf{p}(\mathbf{x}_1), w_{2,i}(\mathbf{x} - \mathbf{x}_2)\mathbf{p}(\mathbf{x}_2), \dots, w_{N_{in},i}(\mathbf{x} - \mathbf{x}_{N_{in}})\mathbf{p}(\mathbf{x}_{N_{in}})]$$

$$\mathbf{S}_{,i}(\mathbf{x}) = \mathbf{A}_{,i}^{-1}[\mathbf{I} - \mathbf{P}\mathbf{Y}(\mathbf{x})] - \mathbf{A}^{-1}\mathbf{P}\mathbf{Y}_{,i}(\mathbf{x})$$

$$\mathbf{Y}_{,i}(\mathbf{x}) = \mathbf{Q}_{,i}^{-1}(\mathbf{x})\mathbf{P}^T\mathbf{A}^{-1}(\mathbf{x}) + \mathbf{Q}^{-1}(\mathbf{x})\mathbf{P}^T\mathbf{A}_{,i}^{-1}(\mathbf{x})$$

$$\mathbf{Q}_{,i}^{-1}(\mathbf{x}) = -\mathbf{Q}^{-1}(\mathbf{x})\mathbf{Q}_{,i}(\mathbf{x})\mathbf{Q}^{-1}(\mathbf{x})$$

$$\mathbf{Q}_{,i}(\mathbf{x}) = \mathbf{P}^T\mathbf{A}_{,i}^{-1}(\mathbf{x})\mathbf{P}$$

$$\mathbf{A}_{,i}^{-1}(\mathbf{x}) = -\mathbf{A}^{-1}(\mathbf{x})\mathbf{A}_{,i}(\mathbf{x})\mathbf{A}^{-1}(\mathbf{x})$$

$$\mathbf{A}_{,i}(\mathbf{x}) = \sum_{l=1}^{N_{in}} w_{l,i}(\mathbf{x} - \mathbf{x}_l)\mathbf{p}(\mathbf{x}_l)\mathbf{p}^T(\mathbf{x}_l) \quad (18)$$

In order to obtain the nontrivial solution of Eq. (12), not only the conditions in normal MLS should be satisfied, in which the nodes for approximation should be well arranged and $N \geq m$ in order to satisfy $\det(\mathbf{A}(\mathbf{x})) \neq 0$, but also $N_b \leq m$ should be satisfied. Especially, if $N = N_b = m$, this formulation degenerates to normal interpolation operation; if $N_{in} = N \geq m$, it degenerates to normal MLS approximation; in general solvable conditions, it can fulfill part interpolation and part approximation in one domain. In an approximation domain $\Omega_{\mathbf{x}}$, if there are some nodes on essential boundary, we can set these nodes as interpolation nodes and set the other nodes as MLS approximation nodes. From Eqs. (12) and (14), it can be easily proved that the shape functions at the interpolation nodes satisfy the property of Kronecker delta property as

$$\Phi_I(\mathbf{x}_J) = \begin{cases} 1 & I = J \\ 0 & I \neq J \end{cases} \quad I = 1, \dots, N; \quad J = N_{in} + 1, \dots, N \quad (19)$$

Thus, the shape function obtained by our new modified MLS procedure can perform Kronecker delta property over the nodes on essential boundary, and the essential boundary can be directly introduced as the methods in FEM without other special treatments. This procedure could also be used in other meshless methods to simplify the introduction of essential boundary conditions.

2.3 MLPG discretization

In this paper, MLPG1, which is based on the local symmetric weak form (LSWF), and uses MLS weight function as the test function in each sub domain, are adopted to implement the discretization of the governing equations.

Integrating the product of Eq. (1) and the test function v_i over the sub domain $\Omega_s \subset \Omega$ (integral domain), we can obtain the local weighted residual integral function (LWRM)

$$\int_{\Omega_s} (\sigma_{ij,j} + b_i - \rho \ddot{u}_i) v_i d\Omega = 0 \quad (20)$$

The compact weight function are used as the trial function v_i (MLPG1), which vanishes over the local boundary L_s ($L_s \cup \Gamma_{su} \cup \Gamma_{st} = \partial\Omega_s = \Gamma_s$, where $\Gamma_{su} = \Gamma_s \cap \Gamma_u$ and $\Gamma_{st} = \Gamma_s \cap \Gamma_t$ are the prescribed displacement and traction boundary within the local domain Ω_s , respectively, but $L_s \cap \Gamma_u = \emptyset$ and $L_s \cap \Gamma_t = \emptyset$). Combining with Eq. (2), Eq. (20) is integrated by parts, which results in the following LSWF expression

$$\int_{\Omega_s} (\rho v_i \ddot{u}_i + v_{i,j} \sigma_{ij} - v_i b_i) d\Omega - \int_{\Gamma_{st}} v_i \bar{t}_i d\Gamma - \int_{\Gamma_{su}} v_i \sigma_{ij} n_j d\Gamma = 0 \quad (21)$$

Substituting Eq. (14) into Eq. (21) yields the sub MLPG discretized equation about node I

$$\mathbf{M}_s \ddot{\mathbf{u}}_s(t) + \mathbf{K}_s \mathbf{u}_s(t) = \mathbf{f}_s(t) \quad (22)$$

where \mathbf{M}_s , \mathbf{K}_s , and \mathbf{f}_s are the local mass, stiffness and load matrices, respectively. The components of the matrices are derived by

$$\begin{aligned} \mathbf{M}_{sIJ} &= \int_{\Omega_s} \rho \phi_J \mathbf{v}(\mathbf{x}, \mathbf{x}_I) d\Omega \\ \mathbf{K}_{sIJ} &= \int_{\Omega_s} \varepsilon_v(\mathbf{x}, \mathbf{x}_I) \mathbf{D} \mathbf{B}_J d\Omega - \int_{\Gamma_{su}} \mathbf{v}(x, x_I) \mathbf{N} \mathbf{D} \mathbf{B}_J \mathbf{S} d\Gamma \\ \mathbf{f}_{sI} &= \int_{\Gamma_{st}} \mathbf{v}(\mathbf{x}, \mathbf{x}_I) \bar{\mathbf{t}} d\Gamma + \int_{\Omega_s} \mathbf{v}(\mathbf{x}, \mathbf{x}_I) \mathbf{b} d\Omega \end{aligned} \quad (23)$$

For 2D elasto-dynamic problems, \mathbf{M}_s is a $2 \times 2N_s$ matrix, \mathbf{K}_s a $2 \times 2N_s$ matrix, where N_s is the bandwidth of \mathbf{K}_s , and \mathbf{f}_s a 2×1 vector. The explicit forms of the matrices in Eqs. (23) are as follows

$$\varepsilon_v = \begin{bmatrix} \varepsilon_{11}^{(1)} & \varepsilon_{22}^{(1)} & 2\varepsilon_{12}^{(1)} \\ \varepsilon_{11}^{(2)} & \varepsilon_{22}^{(2)} & 2\varepsilon_{12}^{(2)} \end{bmatrix}, \quad \mathbf{v} = \begin{bmatrix} w_I & 0 \\ 0 & w_I \end{bmatrix},$$

$$\mathbf{B}_J = \begin{bmatrix} \phi_{J,1} & 0 \\ 0 & \phi_{J,2} \\ \phi_{J,2} & \phi_{J,1} \end{bmatrix}, \quad \mathbf{N} = \begin{bmatrix} n_1 & 0 & n_2 \\ 0 & n_2 & n_1 \end{bmatrix},$$

$$\mathbf{D} = \frac{\bar{E}}{1 - \bar{\nu}^2} \begin{bmatrix} 1 & \bar{\nu} & 0 \\ \bar{\nu} & 1 & 0 \\ 0 & 0 & (1 - \bar{\nu})/2 \end{bmatrix},$$

$$\bar{E} = \begin{cases} E & \text{for plane stress deformations,} \\ E/(1 - \nu^2) & \text{for plane strain deformations,} \end{cases}$$

$$\bar{\nu} = \begin{cases} \nu & \text{for plane stress deformations,} \\ \nu/(1 - \nu) & \text{for plane strain deformations,} \end{cases}$$

$$S_i = \begin{cases} 1 & \text{if } x \in \Gamma_u, \\ 0 & \text{if } x \notin \Gamma_u, \end{cases} \quad (24)$$

where E is the Young's modulus, and ν the Poisson's ratio. In this paper, the sub domain Ω_s is a circle domain, denoted as $\Omega_I(r_{sI})$, with node I as its center. The test function is taken as a spline weight function $w_I = w(x - \mathbf{x}_I)$ in Eq. (8), and has the same center as the sub domain. However, the radius r_{sI} for the test function v over domain Ω_s and the radius r_I for trial function over domain Ω_x , in which the modified MLS approximation is performed, could be chosen differently. Considering the propagation characteristic of the stress waves, lumped mass matrix is used by row-sum technique. Thus Eq. (22) is modified to

$$\bar{\mathbf{M}}_s \ddot{\mathbf{u}}_s(t) + \mathbf{K}_s \mathbf{u}_s(t) = \mathbf{f}_s(t) \quad (25)$$

where

$$\begin{cases} \bar{M}_{sIJ} = \sum_K M_{sIK} & I = J \\ M_{sIJ} = 0 & I \neq J \end{cases} \quad (26)$$

are the lumped mass matrix.

If the node numbers in the whole domain Ω is n , the n sets of Eq. (25) form a global second-time ordinary differential equation system

$$\mathbf{M} \ddot{\mathbf{u}}(t) + \mathbf{K} \mathbf{u}(t) = \mathbf{f}(t) \quad (27)$$

where $\mathbf{u}(t)$ is the displacement vector of the nodes, \mathbf{M} the total diagonalized lump mass matrix, \mathbf{K} the total stiffness matrix, and $\mathbf{f}(t)$ the total load vector. In the practice, for a node I on the essential boundary, considering the prescribed displacements are already known, the corresponding equations in Eq. (27) along this direction need

not to be solved again. The displacement values are directly used in the other equation solutions. This treatment is called direct row cross-out method, which reduces the equation numbers to be solved and increases the calculating efficiency.

2.4 Explicit time integral scheme and its stability conditions

Equation (27) can be solved by central difference scheme [Belytschko, Liu and Moran (2000)],

$$\mathbf{u}^{n+1} = \mathbf{u}^n + \Delta t \mathbf{v}^{n+1/2}, \mathbf{v}^{n+1/2} = \mathbf{v}^{n-1/2} + \Delta t \mathbf{a}^n \quad (28)$$

where \mathbf{u}^{n+1} , \mathbf{u}^n are the displacement vectors at time $t + \Delta t$ and t , $\mathbf{v}^{n+1/2}$ and $\mathbf{v}^{n-1/2}$ are the velocity vectors at time $t + \Delta t/2$ and $t - \Delta t/2$, \mathbf{a}^n is the acceleration vector at time t , Δt is the time increment. This explicit scheme is conditionally stable. The stability condition for algorithm (28) is given by

$$\Delta t \omega_{\max} \leq 2 \quad (29)$$

where $\omega_{\max} = (\lambda_{\max})^{1/2}$, λ_{\max} is the maximum eigenvalue of the matrix

$$\mathbf{K}x = \lambda \mathbf{M}x \quad (30)$$

3 Crack modeling and evaluation method for dynamic fracture parameters

3.1 Treatment of a crack

Because a crack has the property that its length is far longer than its width, from the mathematic point of view, in 2D case, it could be considered as a curve separating two parts of a body, which is also called inner boundary. Different from the treatment of cracks in finite element method, where tremendous remeshing is needed to hold the consistency of mesh boundaries near a crack, in meshless methods, a curved crack could be constructed by several continuous connected line segments. These short crack lines control the approximation domain of a given point. If a crack needs to develop to a certain direction, it is simple to add a crack tip point in that direction, and form a new crack line. Moreover, it is also easy to add, eliminate or split points near a crack tip for a reasonable precision.

Several procedures have been introduced to present this approximation discontinuity, such as visibility criterion

[Belytschko, Gu and Lu (1994)], diffraction or transparency method [Organ, Fleming, Terry and Belytschko (1996)] and see through method [Terry (1994)]. In the present study, visibility criterion is used. The basic idea is that the cracks are assumed to be opaque. When putting a light on an approximation point, within its approximation region, only the nodes that could be lighted are chosen as the basic nodes to perform the approximation. In the practice, we first draw a line between a point to be approximated and a node. If it does not intersect with the crack, this node is then used to approximate the integral point. When considering the crack propagation along a certain direction, a new crack tip point could be added in that direction. Thus the local stiffness, mass and load matrices \mathbf{K}_s , \mathbf{M}_s and \mathbf{f}_s in Eq. (25) should be updated. In favor of the local feature of the present MLPG method, these changes can be made only among the nodes that the added crack line influences. Thus only a small part of the matrices will be changed. This treatment dramatically improves the efficiency of the present algorithm.

3.2 Path-independent dynamic J' integral and evaluation of DSIF

In this paper, the path-independent dynamic J' integral proposed by Nishioka and Atluri (1983) is used to extract the dynamic fracture parameters, for it has good properties of integral path independency, and presents physical meaning of dynamic energy release rate. It is expressed as

$$J'_k = \lim_{\epsilon \rightarrow 0} \left\{ \int_{\Gamma_p + \Gamma_c} [(W + K)n_k - t_i u_{i,k}] dS + \int_{V_p - V_\epsilon} [(\rho \ddot{u}_i - b_i)u_{i,k} - \rho \dot{u}_i \dot{u}_{i,k}] dV \right\} \quad (31)$$

where n_i denotes the outward direction cosine, W and K are the strain and kinetic energy densities. V_p and V_ϵ are the region surrounded by Γ_p and Γ_ϵ , with Γ_ϵ , Γ_p and Γ_c a near-field path, far-field path and crack surface path, respectively, as shown in Figure 1.

In this paper, the far-field path Γ_p is taken as a circle centered at the crack tip with radius $tipR$, and assumed that the gap of a crack is wide enough so that the two surfaces of the crack would not contact with each other during the loading time. Considering the nature boundary condition

4 Numerical examples and discussion

In order to verify the availability of the present algorithm for the dynamic crack problems, some numerical results are discussed in this section. In the practice, quadratic basis and Gaussian weight function are adopted to ensure the accuracy of calculation. The region of the local test function with a spline type (as in Eqn. (8)) Ω_s is taken as a circle centered at node I with a radius r_{Ω_s} , which forms the sub equation system shown in Eq. (25). The radius of the influence domain of MLS interpolation r_I and the integral domain r_{Ω_s} are set differently as $r_I = 2.5 \Delta x$ and $r_{\Omega_s} = 1.1 \Delta x$, where Δx is the smallest space step of the regularly arranged nodes. The other parameters in Eq. (7) is set as $c_I = 0.365 r_I$, and $k = 2$.

A piecewise midpoint quadrature rule [De and Bathe (2001)] is used in the numerical integral of Eqs. (23) and (31). The simple formulation of this integral procedure is as follows: the integral of a function $f(x, y)$ over a sector Ω_{R_0} , which is with radius R_0 , center point (x_0, y_0) , initial angle θ_{init} and total angle θ_0 , is approximated as

$$\int \int_{\Omega_{R_0}} f(x, y) dx dy \approx \sum_{i=1}^{n_\theta} \sum_{j=1}^{n_r} D_{ij} f(x_0 + r_j \cos \theta_i, y_0 + r_j \sin \theta_i) \quad (39)$$

where n_θ and n_r are the numbers of sections subdivided along circular direction and radial direction, $\theta_i = \theta_{init} + (i - 1/2) \Delta \theta (i = 1 \dots n_\theta)$, $r_j = \frac{j^2 - j + 1/3}{j - 1/2} \Delta r (j = 1 \dots n_r)$, $\Delta \theta = \frac{\theta_0}{n_\theta}$ and $\Delta r = \frac{R_0}{n_r}$. This scheme is proved to be superior to other integral schemes numerically, such as Gauss-Legendre product rule, in both stability and efficiency on the condition of similar numerical integral in meshless methods. For detail information, please refer the paper. In the practice, the circle or sector for integral in Eq. (23) is subdivided by 5 in radius direction and 8 in circumferential direction, respectively. 8 quadrature points with uniform separation are used for the integral along each boundary line within a sub-domain. As for the path-independent dynamic J' integral in Eq. (31), 8 by 8 quadrature points are used for the area integral, and 16 quadrature points with uniform separation are used for the line integral.

4.1 Analysis of pure mode problems

Firstly, the dynamic response of a rectangular plate with a centrally located horizontal crack is investigated. For

mode I and II, the tensile stress $\sigma(t) = H(t) \sigma_0$ and in-plane shear stress $\tau(t) = H(t) \tau_0$ are applied along the upper and lower boundaries of the plate, respectively, where $H(t)$ is a Heaviside function. The size of the rectangular plate is 104mm in width and 40mm in height. A half part of this model is drawn in Figure 2, which shows the scattered node pattern and the circle path centered at the crack tip for the calculation of dynamic J' integral.

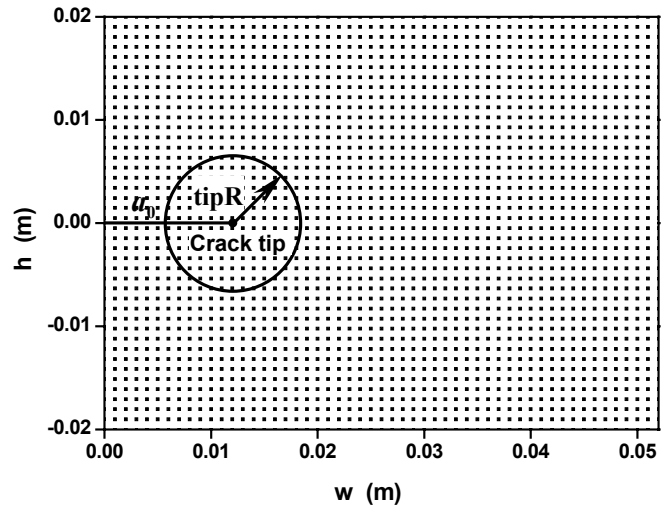


Figure 2 : Discrete model for a plate with a center crack and the path for the dynamic J' integral.

The material parameters are given in Table 1. 4410 nodes with regular pattern (105×42) are used in this analysis. The amplitude of the loading is $\tau_0 = \sigma_0 = 0.1$ MPa. The time step is $\Delta t = 0.1 \mu s$.

Table 1 : Parameters for the calculation of pure and mixed modes DSIF

Crack modes	I	II	Mixed mode
Young's modulus E (GPa)	75.6	73.5	75.6
Poisson's ratio ν	0.286	0.25	0.286
Density ρ (kg/m ³)	2450	2450	2450
Crack length a_0 (mm)	12	12	22.63
Node number	4410	4410	1485

Figures 3 and 4 show the path independence of J_1^0 integrals for modes I and II, and they are path independent to within 2.4% and 1.8% of the values for path tipR = 3mm, respectively. Figures 5 and 6 describe the normalized dynamic stress intensity factors $K_I(t) / (\sigma_0 \sqrt{\pi a_0})$

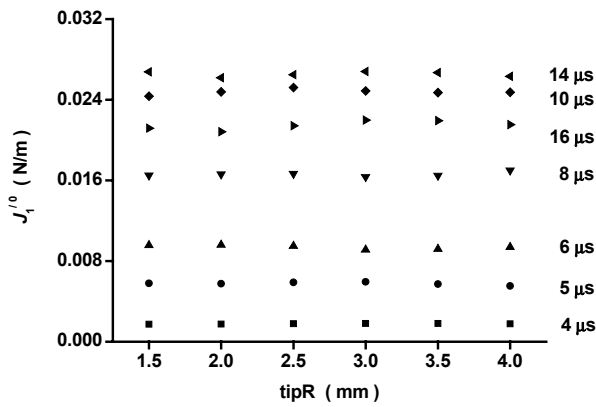


Figure 3 : Path-independence of dynamic J_1^0 integral computed by present algorithm for pure mode I (with a stationary crack).

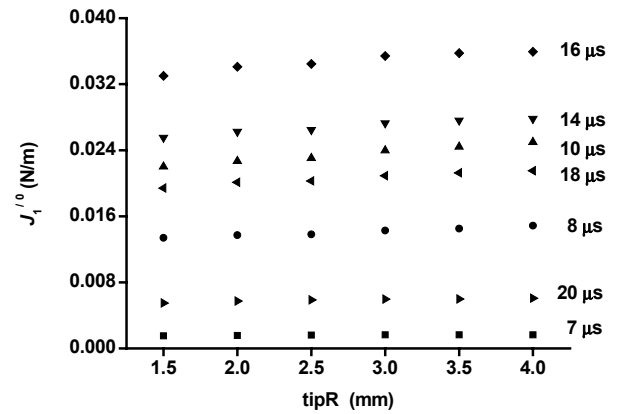


Figure 4 : Path-independence of dynamic J_1^0 integral computed by present algorithm for pure mode II (with a stationary crack).

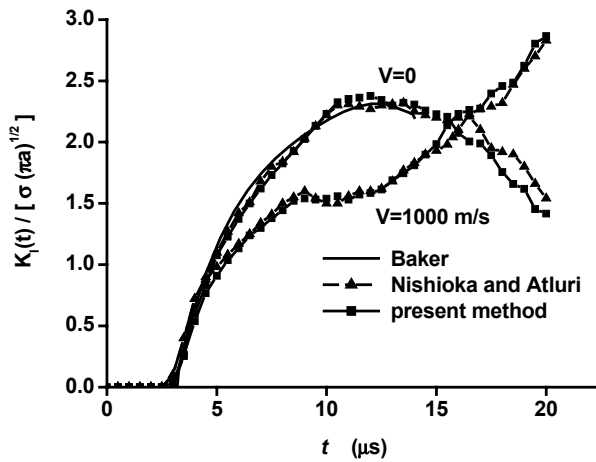


Figure 5 : Time-dependence of the normalized mode I dynamic stress intensity factors for a center-cracked rectangular plate subjected to Heaviside step-function normal stress (with a stationary crack and a propagating crack at a constant crack velocity $V = 1000$ m/s, respectively).

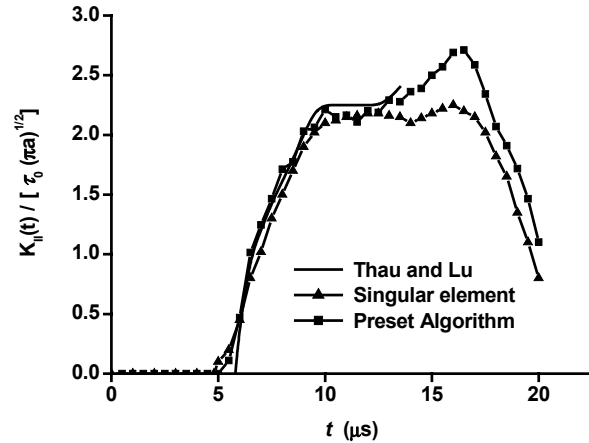


Figure 6 : Time-dependence of the mode II dynamic stress intensity factors for a center-cracked rectangular plate subjected to Heaviside step-function shear stress (with a stationary crack).

and $K_{II}(t)/(\tau_0\sqrt{\pi a_0})$ for modes I (with a stationary crack and a propagating crack at a constant crack velocity $V = 1000$ m/s, respectively) and II (with a stationary crack).

These results agree well with the analytical solutions [Baker (1962); Thau and Lu (1971)], and the numerical results computed by moving singular elements [Nishioka and Atluri (1980)] and singular elements [Kishimoto, Aoki and Sakata (1980)], respectively.

4.2 Analysis of mixed mode problem

Figure 7 shows the scattered node pattern of a rectangular plate with a crack slanted at 45° . 1485 nodes with regular pattern (45×33) are used in this analysis. A tensile stress $\sigma(t) = H(t) \sigma_0$ is applied on the left boundary and the hinged supports are posed on the other three boundaries. The loading amplitude is $\sigma_0 = 0.1$ MPa. The crack is from (6.5, 0) to (22.5, 16). The other computational conditions are shown in Table 1.

Figures 8 and 9 are the path independence of J_1^0 and J_2^0 integrals for mixed mode, respectively. Referring to the

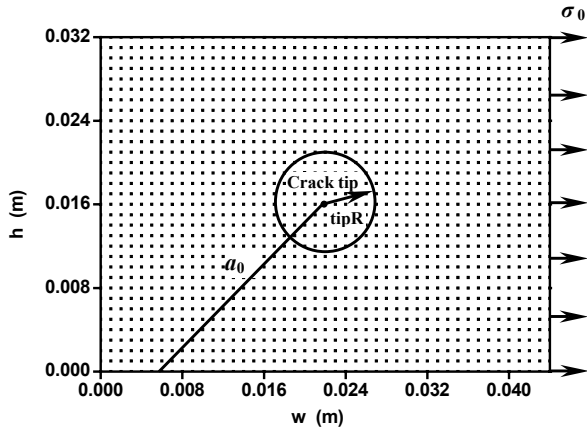


Figure 7 : Discrete model for a plate with a crack slanted at 45° and the path for the dynamic J' integrals.

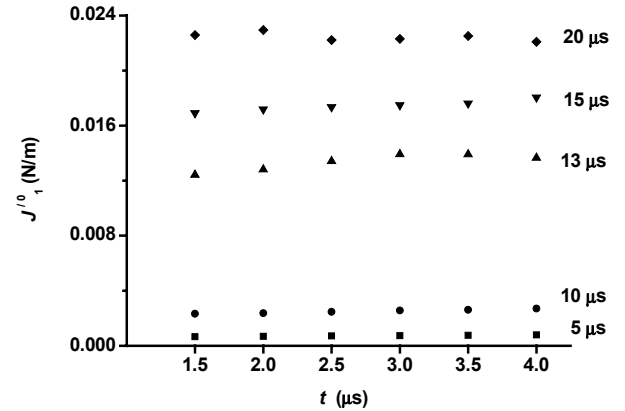


Figure 8 : Path-independence of dynamic J_1^0 integral computed by present algorithm for mixed mode.

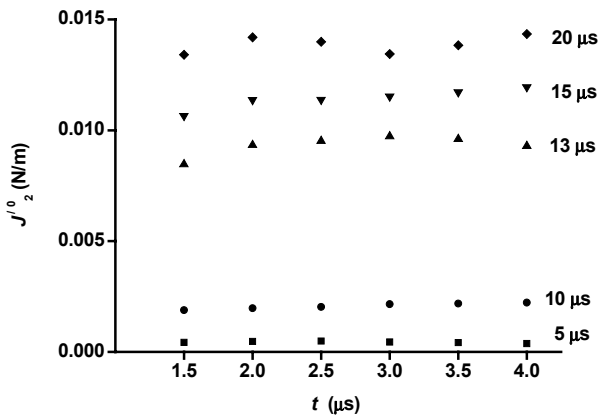


Figure 9 : Path-independence of dynamic J_2^0 integral computed by present algorithm for mixed mode.

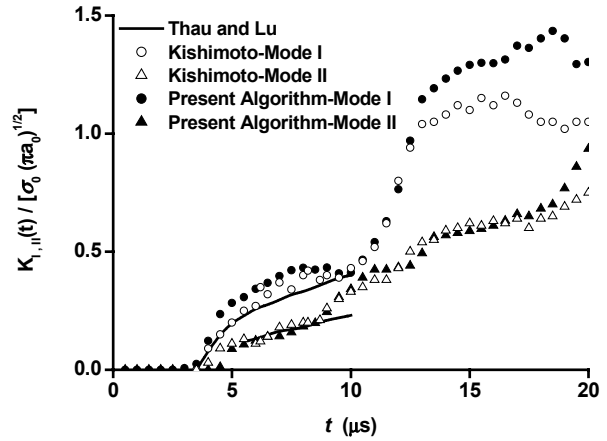


Figure 10 : Time-dependence of the normalized mixed mode dynamic stress intensity factors for a rectangular plate with a slanted crack.

values at tipR=3mm, the variation of the path independent J_1^0 and J_2^0 are within 0.6% and 3.1%, respectively.

Figure 10 shows the results for the normalized dynamic stress intensity factors $K_I(t)/(\sigma_0\sqrt{\pi a_0})$ and $K_{II}(t)/(\sigma_0\sqrt{\pi a_0})$. Comparing these results with the analytical solutions [Thau and Lu (1971)], and the numerical results computed by singular finite element [Kishimoto, Aoki and Sakata (1980)], they agree well.

4.3 Stress wave diffraction in a square plate with cracks

In this section, the stress wave propagation and diffraction near the cracks are investigated. Figures 11a, 11b and 11c exhibit the diagrammatic sketches of a plate

(200mm \times 200mm) without cracks, with a horizontal crack or a vertical crack, respectively.

A uniform impact load with $b = 8$ mm in length is applied on the center of the upper surface of the square plate. The impact load is expressed as

$$\begin{cases} \sigma_x = \sigma_y = \sigma_{xy} = 0, v_x = v_y = 0 & \text{for } t = 0 \\ \sigma_y = p_0 [1 - 0.5(10^6 t - 2.5)^2] \exp[-(10^6 t - 2.5)^2], \\ \sigma_{xy} = 0 & \text{for } y = 0 \end{cases} \quad (40)$$

where $p_0 = 1$ MPa. The crack length is $a = 40$ mm. The location of the cracks is shown in Figures 12-14 in detail. The material parameters are: $E = 210$ MPa, $\nu = 0.3$ and $\rho = 7800$ kg/m³. 40401 nodes with a regular pattern

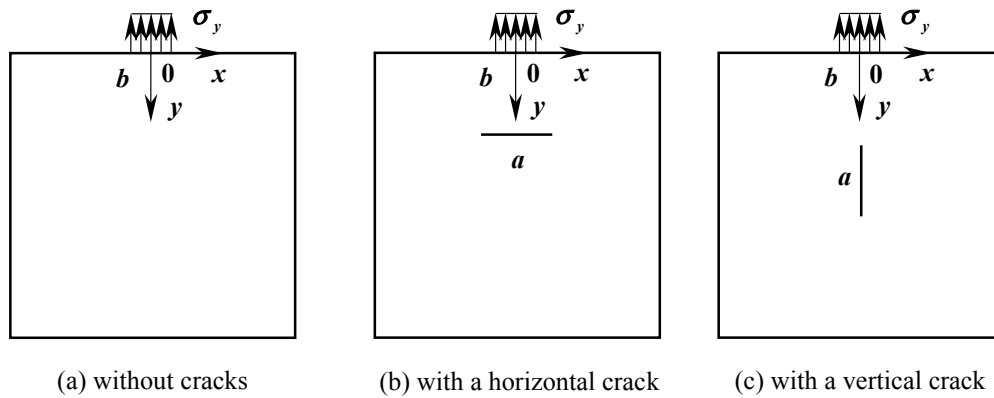


Figure 11 : Diagrammatic sketches of a plate without cracks, with a horizontal crack or a vertical crack.

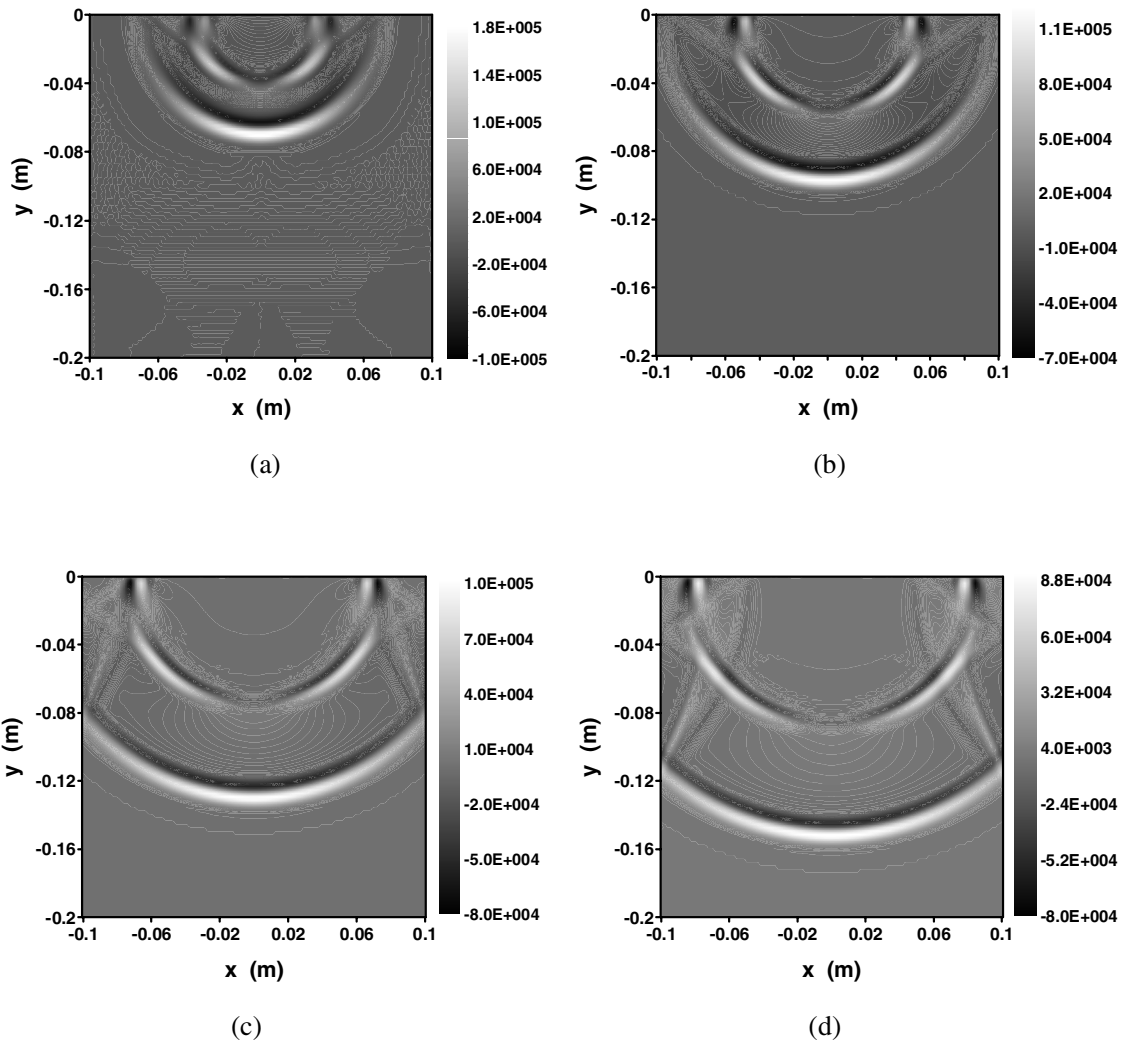


Figure 12 : The stress wave field of σ_y at four different times (no cracks). Figures (a), (b), (c) and (d) are for propagation times 15, 20, 26 and 30 μs , respectively.

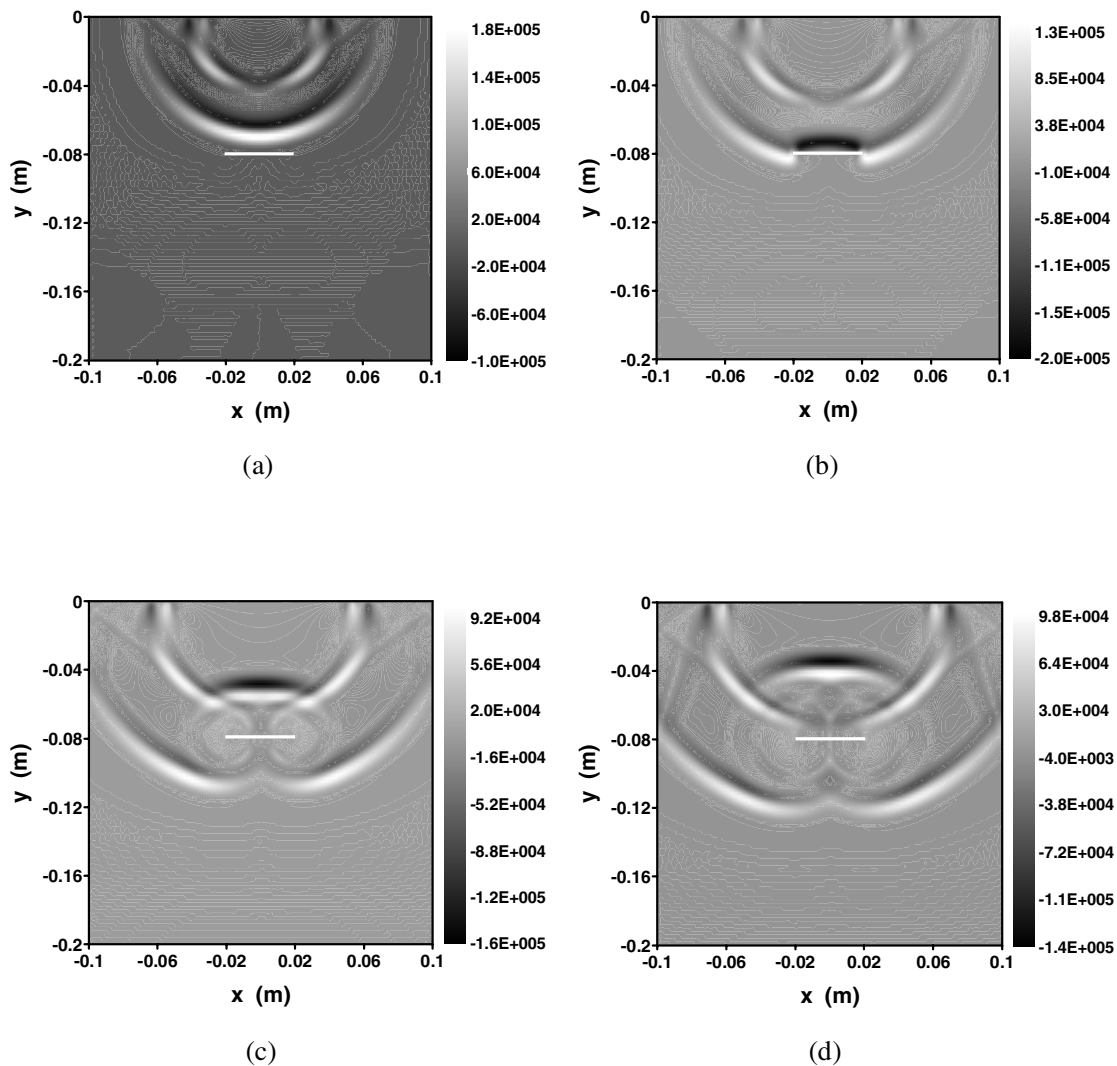


Figure 13 : The stress wave field of σ_y at four different times (central horizontal cracks). Figures (a), (b), (c) and (d) are for propagation times 15, 18, 22.5 and 25 μs , respectively.

(1mm \times 1mm in a space step) are adopted in this example. The time step is also $\Delta t = 0.1 \mu s$.

Figures 13 and 14 display the stress wave propagation processes in the square plate with a horizontally or vertically located crack under the impact loading at different time, respectively. In order to make a comparison, the stress wave propagation process in the same plate without cracks is also given in Figure 12. Figures 12a, 13a and 14a are the stress wave field at time $t = 15 \mu s$. The longitudinal wave, shear wave, Rayleigh wave and von Schmidt wave are distinctly demonstrated. It can be observed clearly that the peak of Rayleigh wave decreases rapidly with the increase of depth. Figures 13b, 13c and

13d show the diffraction process of the waves due to horizontal crack continuously. From Figure 13b ($t = 18 \mu s$), it can be seen that the longitudinal wave is reflected on the upper surface of the crack, and it changes from the tension wave to the pressure wave. At the same time, the diffraction of the longitudinal wave at two crack tips happens. At $t = 22.5 \mu s$ and $t = 25 \mu s$ (shown in Figures. 13c and 13d, respectively), two kinds of diffracted waves at the two crack tips have radiated out, and according to their wave velocities, it could be identified that they are longitudinal wave and shear wave, respectively.

As shown in Figure 14, for the case of the vertical crack, the diffracted waves from the upper crack tip are not so

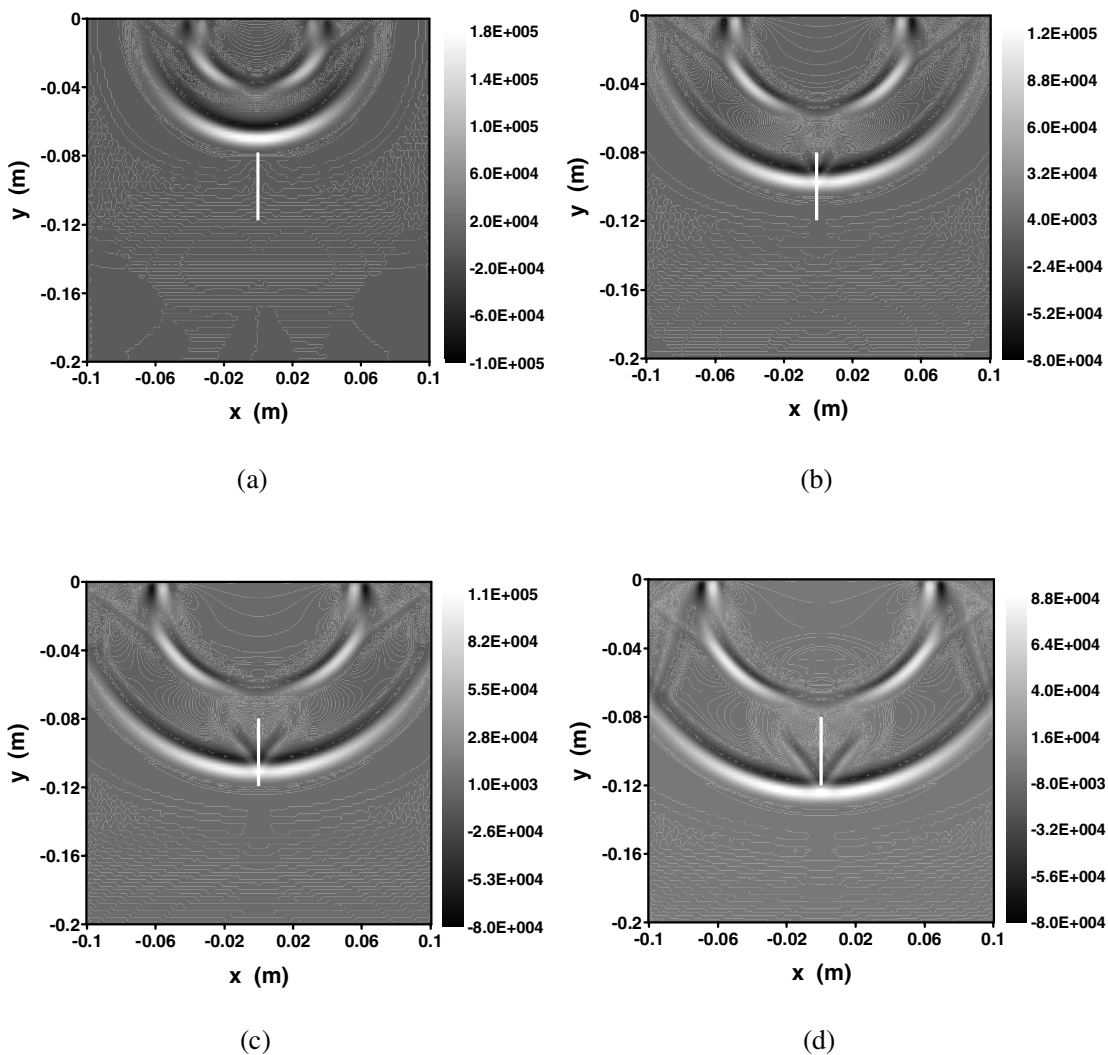


Figure 14 : The stress wave field of σ_y at four different times (central vertical cracks). Figures (a), (b), (c) and (d) are for propagation times 15, 20, 22.5 and 25 μs , respectively.

clear, for the reason that the width of the crack is too small. When the longitudinal wave arrives at the vertical crack and then propagates along the crack, two head waves start to appear in Figure 14b ($t = 20 \mu s$), which are produced by the grazing incidence of the longitudinal wave over two surfaces of the crack. These two head waves propagating at the velocity of the shear wave c_s are clearly displayed in Figures 14c ($t = 22.5 \mu s$) and 14d ($t = 25 \mu s$), respectively.

The above numerical results demonstrate high capability of the present algorithm in the extraction of the complicated stress wave fields, such as the perplexing reflection and diffraction phenomena caused by cracks.

5 Conclusions

A new MLPG algorithm is proposed to analyze stress wave propagation and dynamic fracture problems in elastic media with cracks. In our algorithm, a new modified MLS procedure is developed for simplifying the treatment of essential boundary condition by introducing Lagrange multiplier into MLS procedure. In addition, lumped mass and explicit central difference scheme are used in this algorithm, which makes the calculation more efficiently. By using this algorithm, the dynamic stress intensity factors for pure modes and mixed modes are evaluated through an indirect method of path-independent dynamic J' integrals. Our results are con-

sistent with the analytical solutions and the results computed by singular finite element method and moving singular FEM. Good agreement is presented. Finally the elastic wave field in a square plate with a crack is investigated. The complicated wave fields caused by the wave diffraction near the crack tips, and the multi-interfaces between different waves are clearly extracted from the results computed by the present algorithm in detail. All the numerical examples given above prove the accuracy, capability and efficiency of present MLPG algorithm in the application of dynamic fracture problems.

Acknowledgement: The authors gratefully acknowledge the financial support of the National Natural Science Foundation of China (grant nos. 10302002 and 10232040). The third author would also thanks for the support of the technological foundation of Beijing Jiaotong university (grant no. 2004RC042).

References

- Atluri, S. N.** (2004): *The Meshless Local-Petrov-Galerkin Method for Domain & BIE Discretizations*, Tech Science Press, 680 pages.
- Atluri, S. N.** (2005): *Methods of Computer Modeling in Engineering & the Sciences-Part I*, Tech Science Press, 560 pages.
- Atluri, S. N.; Han, Z. D.; Rajendran, A. M.** (2004): A new implementation of the meshless finite volume method, through the MLPG "Mixed" approach, *CMES: Computer Modeling in Engineering & Sciences*, vol. 6, no. 6, pp. 491-513.
- Atluri, S. N.; Shen, S.** (2002): *The Meshless Local Petrov-Galerkin (MLPG) Method*, Tech Science Press, 429 pages.
- Atluri, S. N.; Zhu, T.** (1998): A new Meshless Local Petrov-Galerkin (MLPG) approach in computational mechanics, *Computational Mechanics*, vol. 22, pp. 117-127.
- Atluri, S. N.; Zhu, T.** (2000): The Meshless Local Petrov-Galerkin (MLPG) approach for solving problems in elasto-statics, *Computational Mechanics*, vol. 25, no. 2-3, pp. 169-179.
- Baker, B. R.** (1962): Dynamic stresses created by a moving crack, *ASME Journal of Applied Mechanics*, vol. 29, pp. 449-545.
- Belytschko, T.; Gu, L.; Lu, Y. Y.** (1994): Fracture and crack growth by element-free Galerkin methods, *Modeling Simulations for Materials Science and Engineering*, vol. 2, pp. 519-534.
- Belytschko, T.; Krougauz, Y.; Organ, D.; Fleming, M.; Krysl, P.** (1996): Meshless method: an overview and recent developments, *Computer Methods in Applied Mechanics and Engineering*, vol. 139, pp. 3-47.
- Belytschko, T.; Liu, W. K.; Moran, B.** (2000): *Non-linear Finite Elements for Continua and Structures*, John Wiley & Son, New York, 666 pages.
- Batra, R. C.; Ching, H. K.** (2002): Analysis of elastodynamic deformations near a crack/notch tip by the Meshless Local Petrov-Galerkin (MLPG) method, *CMES: Computer Modeling in Engineering & Sciences*, vol. 3, no. 6, pp. 717-730.
- Ching, H. K.; Batra, R. C.** (2001): Determination of crack tip fields in linear elastostatics by the Meshless Local Petrov-Galerkin (MLPG) method, *CMES: Computer Modeling in Engineering & Sciences*, vol. 2, no. 2, pp. 273-289.
- De, S.; Bathe, K. J.** (2001): The method of finite spheres with improved numerical integration, *Computers and Structures*, vol. 79, no. 22-25, pp. 2183-2196.
- Freund, L. B.** (1990): *Dynamic Fracture Mechanics*, Cambridge University Press, 563 pages.
- Gingold, R. A.; Moraghan, J. J.** (1977): Smoothed particle hydrodynamics: theory and applications to non-spherical stars, *Mon. Not. Roy. Astrou. Soc.*, vol. 18, pp. 375-389.
- Gu, Y. T.; Liu, G. R.** (2001): A Meshless Local Petrov-Galerkin (MLPG) method for free and forced vibration analyses for solids, *Computational Mechanics*, vol. 27, no. 3, pp. 188-198.
- Han, Z. D.; Atluri, S. N.** (2004): A Meshless Local Petrov-Galerkin (MLPG) approach for 3-dimensional elasto-dynamics, *CMC-COMPUTERS MATERIALS & CONTINUA*, vol. 1, no. 2, pp. 129-140.
- Kishimoto, K.; Aoki, S.; Sakata, M.** (1980): Dynamic Stress Intensity Factors using *J*-integral and Finite Element Method, *Engineering Fracture Mechanics*, vol. 13, pp. 387-394.
- Lancaster, P.; Salkauskas, K.** (1981): Surfaces generated by moving least squares methods, *Mathematics of Computation*, vol. 37, no. 155, pp. 141-158.

- Li, S.; Liu, W. K.** (2002): Meshfree and particle methods and their applications, *ASME Applied Mechanics Review*, vol. 55, no. 1, pp. 1-34.
- Lin H.; Atluri S. N.** (2000): Meshless Local Petrov-Galerkin (MLPG) method for convection-diffusion problems, *CMES: Computer Modeling in Engineering & Sciences*, vol. 1, no. 2, pp. 45-60.
- Liu, G. R.** (2002): *Mesh Free Methods: Moving Beyond the Finite Element Method*, CRC press, 692 pages.
- Long S. Y.; Atluri S. N.** (2002): A Meshless Local Petrov-Galerkin method for solving the bending problem of a thin plate, *CMES: Computer Modeling in Engineering & Sciences*, vol. 3, no. 1, pp. 53-63.
- Melen, J. M.; Babuska, I.** (1996): The partition of unity finite element method: basic theory and application, *Computer Methods in Applied Mechanics and Engineering*, vol. 139, pp. 289-314.
- Nishioka, T.; Atluri, S. N.** (1980): Numerical modeling of dynamic crack propagation in finite bodies, by moving singular elements –part II. Results, *Journal of Applied Mechanics*, vol. 47, no. 3, pp. 577-582.
- Nishioka, T.; Atluri, S. N.** (1983): Path independent integrals, energy release rates and general solutions of near-tip fields in mixed-mode dynamic fracture mechanics, *Engineering Fracture Mechanics*, vol. 18, no. 1, pp. 1-22.
- Organ, D.; Fleming, M.; Terry, T.; Belytschko, T.** (1996): Continuous meshless approximations for non-convex bodies by diffraction and transparency, *Computational Mechanics*, vol. 18, pp. 1-11.
- Powell, M. D. J.** (1992): The theory of radial basis function approximation in 1990, *Advances in Numerical Analysis Vol. II: Wavelets, Subdivision Algorithms and Radial Basis Functions*, Clarendon Press, Oxford, vol. 2, pp. 105-210.
- Qian, L. F.; Batra, R. C.; Chen, L. M.** (2004): Static and dynamic deformations of thick functionally graded elastic plates by using higher-order shear and normal deformable plate theory and Meshless Local Petrov-Galerkin method, *Composites: Part B*, vol. 35, no. 6-8, pp. 685-697.
- Rosakis, A. J.; Ravichandran, G.** (2000): Dynamic failure mechanics, *International Journal of Solids and Structures*, vol. 37, no. 1-2, pp.331-348.
- Terry, T. G.** (1994): *Fatigue crack propagation modeling using the element-free Galerkin method*, Master's thesis, Northwestern University.
- Thau, S. A.; Lu, T. H.** (1971): Transient stress intensity factors for a finite crack in an elastic solid caused by a dilatational wave, *International Journal of Solids and Structures*, vol. 7, no. 7, pp. 731-750.

